

Polarity tuning of spin-orbit-induced spin splitting in two-dimensional transition metal dichalcogenides

Moh. Adhib Ulil Absor,^{1, a)} Iman Santosa,¹ Harsojo,¹ Kamsul Abraha,¹ Hiroki Kotaka,² Fumiyuki Ishii,³ and Mineo Saito³

¹⁾*Department of Physics, Universitas Gadjah Mada BLS 21 Yogyakarta Indonesia.*

²⁾*Elements Strategy Initiative for Catalysts and Batteries (ESICB),
Kyoto University, Kyoto 615-8520, Japan*

³⁾*Faculty of Mathematics and Physics Institute of Science and Engineering
Kanazawa University 920-1192 Kanazawa Japan.*

(Dated: 28 June 2021)

The established spin splitting in monolayer (ML) of transition metal dichalcogenides (TMDs) that is caused by inversion symmetry breaking is dictated by mirror symmetry operations to exhibit fully out-of-plane direction of spin polarization. Through first-principles density functional theory calculations, we show that polarity-induced mirror symmetry breaking leads to sizable spin splitting having in-plane spin polarization. These splittings are effectively controlled by tuning the polarity using biaxial strain. Furthermore, the admixtures of the out-of-plane and in-plane spin-polarized states in the strained polar systems are identified, which is expected to influence the spin relaxation through the Dyakonov-Perel mechanism. Our study clarified that the polarity-induced mirror symmetry breaking plays an important role in controlling the spin splitting and spin relaxation in the TMDs ML, which is useful for designing future spintronic devices.

PACS numbers: Valid PACS appear here

Keywords: Suggested keywords

^{a)}Electronic mail: adib@ugm.ac.id

I. INTRODUCTION

Exploration of spin-orbit coupled systems is now at the heart of the growing research field of spintronics that focuses on the manipulation of non-equilibrium material properties using spin-orbit coupling (SOC). The SOC is a relativistic interaction arising from electrons movement in the nuclear electric field, which allows for generation and manipulation of electron spin¹. Current-induced spin polarization² and the spin Hall effect³ are important examples of spintronics phenomena where the SOC plays an important role. For spintronics device operation, semiconducting structures are promising because of their manipulability under gate voltages^{4,5}. However, a stable two-dimensional (2D) thin film is highly desirable, which is advantageous for circuit integration. Here, some attentions are given for the 2D materials such as graphene⁶ and their analogs like silicene and germanene⁷ due to their exotic properties such as high carrier mobility and long spin lifetime⁸⁻¹⁰. However, the weak SOC effect in these materials^{8,9} may limit their functionality for spintronic applications.

Recently, monolayer (ML) of transition metal dichalcogenides (TMDs), a new class of the 2D materials, has attracted much attention because of their extraordinary properties, especially the exotic spin-valley coupled electronic structures that promise future spintronic and valleytronic applications¹¹⁻¹⁸. The bulk phase of the TMDs systems is characterized by an inversion symmetric of $2H$ MX_2 stacking orders with space group D_{6h}^{19} . In the ML phase, the inversion symmetry is broken, leading to the fact that the symmetry reduces to be $D_{3h}^{14,17}$. This inversion symmetry breaking together with strong SOC in the $5d$ orbitals of transition metals atoms give rise to large spin splitting^{13,14,16,17,20}, which plays an important role in inducing some of interesting phenomena such as spin Hall effect^{21,22}, spin- and valley-dependent selection rule for optical transitions¹⁸, and magnetoelectric effect²³. Furthermore, in the D_{3h} point group symmetry, mirror symmetry operation on the surface plane of the MX_2 ML suppresses the spin splitting to exhibit fully out-of-plane spin polarization, which is believed to be responsible for inducing strongly enhanced spin relaxation through Dyakonov-Perel mechanism^{14,17,24,25}. Previous experimental studies have confirmed that long-lived spin relaxation and spin coherence of electrons have been reported on various MX_2 ML such as MoS₂ ML^{24,25} and WS₂ ML²⁵.

Because the mirror symmetry in the surface plane of the MX_2 ML plays a significant role in controlling the spin splitting and spin-polarized states, new electronic properties

are expected to appear by breaking this mirror symmetry. Such situation is achieved by introducing the polar structures MXY ^{26,27}, in which the polarity that is induced by out-of-plane distance difference between transition metal (M) and chalcogen (X,Y) atoms breaks the mirror symmetry in the surface plane. Experimentally, it is possible to create such polar structures by growth on the polar substrate by recently developed molecular beam epitaxial (MBE) technique^{28,29}. This is supported by the fact that the stability of various polar MXY ML structures such as the polar WSSe and MoSSe MLs has recently been reported^{26,27}. However, due to the structural-dependent of the polarity, controlled changes in the polar structure, for example by applying strain, effectively tunes the polarity, which is expected to induce useful properties for spintronics.

In this paper, we perform first-principles density functional theory calculations to clarify the polarity-strain dependent on the electronic properties of the TMDs ML. We find that in addition to the established spin splitting having fully-out-of-plane spin polarization, a sizable spin splitting exhibiting in-plane spin polarization is observed in the polar MXY ML. These splittings are found to be effectively controlled by tuning the polarity, which is achieved by applying biaxial strain. The origin of the spin splitting and spin-polarized states is analyzed on the basis of symmetry arguments combined with orbital hybridization analyses. Furthermore, the admixtures of the out-of-plane and in-plane spin-polarized states in the strained polar systems are identified, and their implications to the spin relaxation are discussed. Finally, the possible applications of our systems for spintronics are discussed.

II. MODEL AND COMPUTATIONAL DETAILS

Similar to the case of the non-polar MX_2 , crystal structure of the polar MXY consists of X - M - Y slabs weakly bonded by van der Waals interaction¹⁹. Here, an intermediate layer of hexagonally arranged the transition metal atoms (M) is sandwiched between two layers of the chalcogenide atoms (X,Y) through strong ionic-covalent bonds forming a trigonal prismatic arrangement. In the bulk phase, both the non-polar MX_2 and polar MXY structures have an inversion symmetric of a $2H$ stacking order with a space group of D_{6h} . However, this inversion symmetry is broken in the monolayer (ML) phase. In the case of the non-polar MX_2 ML, its symmetry reduces to be D_{3h} . This symmetry consists of a threefold rotation C_3 around the trigonal z axis and two mirror symmetry operations with respect to the $x - y$

plane (M_{x-y}) and the $y-z$ plane (M_{y-z}) [Fig. 1(a)]. On the contrary, the mirror symmetry M_{x-y} is broken in the case of the polar MXY ML, leading to the fact that the symmetry becomes C_{3v} [Fig. 1(b)]. The broken of mirror symmetry M_{x-y} in the polar MXY ML is induced by the polarity originated from the out-of-plane interlayer distance difference, Δd_{\perp} . Here, Δd_{\perp} is defined as $\Delta d_{\perp} = |d_{\perp(M-Y)} - d_{\perp(M-X)}|$, where $d_{\perp(M-X)}$ and $d_{\perp(M-Y)}$ are the distance between M atoms and X or Y atoms in the out-of-plane direction. Because the physics in the polar MXY and non-polar MX_2 ML systems are essentially the same for the group- VI transition metal dichalcogenides (TMDs), we here choose WSSe and WS₂ MLs as an example of the polar MXY and non-polar MX_2 MLs, respectively.

We performed first-principles electronic structure calculations based on the density functional theory (DFT) within the generalized gradient approximation (GGA)³⁰ using the OpenMX code³¹. We used norm-conserving pseudopotentials³², and the wave functions are expanded by the linear combination of multiple pseudoatomic orbitals (LCPAOs) generated using a confinement scheme^{33,34}. The orbitals are specified by W7.0- $s^2p^2d^2f^1$, S9.0- $s^2p^2d^1$, and Se9.0- $s^2p^2d^1$, which means that the cutoff radii are 7.0, 9.0, and 9.0 bohr for the W, S, and Se atoms, respectively, in the confinement scheme^{33,34}. For the W atoms, two primitive orbitals expand the s , p , and d orbitals, and one primitive orbital expands the f orbital. On the other hand, for the S and Se atoms, two primitive orbitals expand the s and p orbitals, and one primitive orbital expands d orbital. The SOC was included in our DFT calculations, and the spin textures in k -space were calculated using the k -space spin density matrix of the spinor wave function^{17,35-38}.

Two dimensional structures of the non-polar MX_2 and polar MXY MLs are modeled as a periodic slab with a sufficiently large vacuum layer (25 Å). The use of the large vacuum layer in the present system is to ensure that the electron density of the material tails off to zero in the vacuum and to avoid interaction between adjacent layers along the direction perpendicular to the surface plane. The geometries were fully relaxed until the force acting on each atom was less than 1 meV/Å. Here, we find that the optimized in-plane lattice constant is 3.24 Å for the case of the polar WSSe ML, which is larger than that of the non-polar WS₂ ML (3.18 Å), but it is in a good agreement with previous results [3.24 Å²⁶ to 3.25 Å²⁷]. Furthermore, we characterize the degree of the polarity in our system by evaluating Δd_{\perp} . In the case of the non-polar WS₂ ML, we find that the calculated value of Δd_{\perp} is zero, indicating that this structure is symmetric, thus, justifying the non-polarity

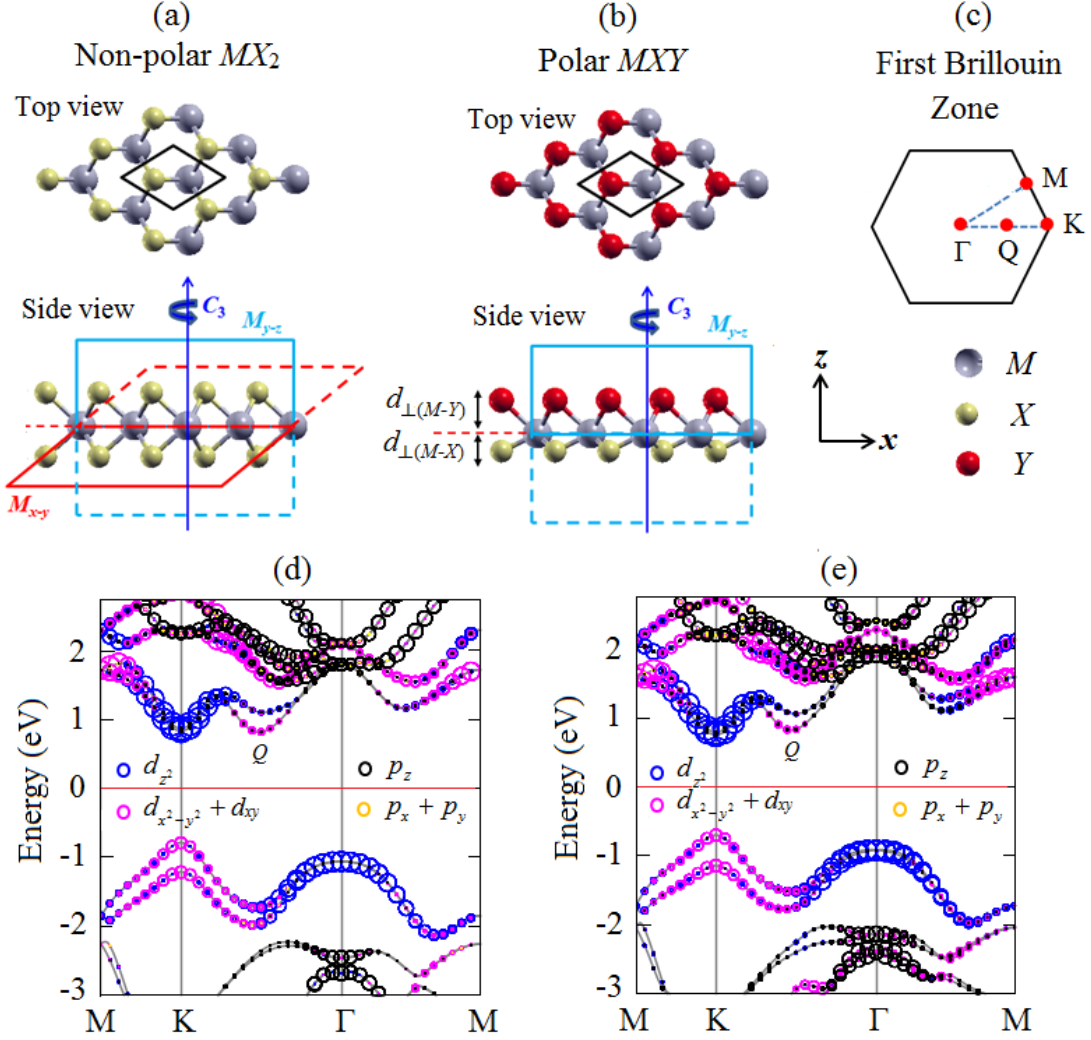


FIG. 1. Top and side views of (a) the non-polar MX_2 and (b) the polar MXY monolayers (MLs) structures. These structures are characterized by a threefold rotation C_3 around the trigonal z axis and two mirror symmetry operations with respect to the $x-y$ plane (M_{x-y}) and to the $y-z$ plane (M_{y-z}). Out-of-plane distance between transition metal (M) and chalcogen atoms (X, Y) [$d_{\perp(M-Y)}$, $d_{\perp(M-X)}$] is indicated. First Brillouin zone, which is specified by the high symmetry points (Γ , K , and M points) is shown. Here, the points located along the Γ - K line, namely the Q point is indicated. Orbital-resolved of the electronic band structures for (c) the non-polar WS_2 ML and (d) the polar $WSSe$ ML. The radius of circles reflects the magnitudes of spectral weight of the particular orbitals to the band. The calculations are performed with inclusion the effect of the spin-orbit coupling.

of this structures. On the contrary, in the case of the polar WSSe ML, it is found that the calculated value of Δd_{\perp} is 0.154 Å, showing that this system is polar. Because of the structural-dependent of Δd_{\perp} , it is expected that the polarity can be controlled by applying strain.

III. RESULT AND DISCUSSION

A. Electronic structures and characteristic of the spin splitting

To investigate the effect of the polarity on the electronic properties of the TMDs ML, we show in Figs. 1(d) and 1(e) orbital-resolved of electronic band structures calculated on the first Brillouin zone [Fig. 1(c)]. In the case of the non-polar WS₂ ML, we observe two local maxima in the valence band maximum (VBM) located on the K and Γ points, which are predominately filled by $d_{x^2-y^2} + d_{xy}$ and d_{z^2} orbitals, respectively [Fig. 1(d)]. On the other hand, in the conduction band minimum (CBM), we identify two local minima with close in energy located on the K point and midway between the Γ and K points, namely the Q points. These local minima at Q and K points are mainly originated from the $d_{x^2-y^2} + d_{xy}$ and d_{z^2} orbitals, respectively [Fig. 1(d)]. Since the VBM and CBM are centered at the K point, a direct band gap with an energy gap of 1.68 eV is observed, which is in good agreement with previous calculations^{17,39}. Similar to the case of the non-polar WS₂ ML, the direct band gap is also identified in the case of the polar WSSe ML [Fig. 1(e)]. However, the energy gap of the polar WSSe ML (1.55 eV) is smaller than that of the non-polar WS₂ ML. Due to the out-of-plane crystal asymmetry in the polar WSSe ML [Fig. 1(b)], hybridization between the out-of-plane orbitals [d_{z^2} , p_z] enhances, resulting in that energy level of the K point in the CBM shifts to be lower than that observed on the non-polar WS₂ ML, thus induces lowering the band gap. These features of electronic band structures are consistent with recent observation of the electronic properties across the TMDs family^{14–17,26}.

Turning the SOC, a spin splitting in the electronic band structures is established in both the non-polar and polar TMDs ML due to the absence of inversion symmetry [Fig. 2]. In the case of the non-polar WS₂ ML, the existence of the mirror symmetry in the surface plane (M_{x-y}) suppresses the spin splitting in the band structures except for \vec{k} point along the Γ - M direction. On the contrary, the mirror symmetry M_{x-y} is broken in the case of the

TABLE I. The calculated value of spin splitting in different high symmetry points in the first Brillouin zone for the VBM and CBM. Here, $\Delta E_{K,\text{VBM}}$ denotes the spin splitting at the K point in the VBM, while $\Delta E_{K,\text{CBM}}$ and $\Delta E_{Q,\text{CBM}}$ denote the spin splitting at the K and Q points in the CBM, respectively. A comparison with previous results are also shown.

Monolayer (ML)	$\Delta E_{K,\text{VBM}}$ (eV)	$\Delta E_{K,\text{CBM}}$ (eV)	$\Delta E_{Q,\text{CBM}}$ (eV)	Reference
Non-polar WS ₂ ML	0.43	0.03	0.33	This work
	0.43	-	-	Ref. ¹⁴
	0.43	0.03	0.33	Ref. ¹⁷
	0.41-0.47	-	-	Ref. ¹⁵
	0.43	0.03	-	Ref. ¹⁶
	0.43	0.03	0.26	Ref. ⁴⁰
Polar WSSe ML	0.25	0.04	0.20	This work
	0.44	0.03	-	Ref. ²⁶

polar WSSe ML, leading to the fact that the spin degeneracy of the bands along the Γ - M direction is lifted. It is noted here that due to time reversability, the spin degeneracy is visible in the Γ and M points. However, at the K and Q points, the time reversal symmetry is broken, inducing Zeeman-like spin splitting¹³.

The calculated values of the spin splitting in different high symmetry points in the first Brillouin zone for the VBM and CBM are summarized in Table I. Consistent with previous studies^{14-17,26,40}, the spin splitting is identified on the K and Q points in the VBM and CBM, respectively. In the case of the polar WSSe ML, large spin splitting up to 0.45 eV is observed on the K point in the VBM, which is comparable with that in the case of the non-polar WS₂ ML ($\Delta E_{K,\text{VBM}} = 0.43$ eV). However, in the Q point of the CBM, the spin splitting in the case of the polar WSSe ML ($\Delta E_{Q,\text{CBM}} = 0.20$ eV) is smaller than that in the case of the non-polar WS₂ ($\Delta E_{Q,\text{CBM}} = 0.33$ eV). Interestingly, a sizable spin splitting around the Γ point in the VBM that is not found in the case of the non-polar WS₂ ML is observed in the case of the polar WSSe ML [Fig. 2]. This splitting is referred as Rashba splitting, which is consistent with that previously reported by Cheng *at al.*²⁶. Because the energy level of the K point is close to that of the Γ point in the VBM, interplay between the Zeeman-like spin splitting in the K point and the Rashba spin splitting around the Γ

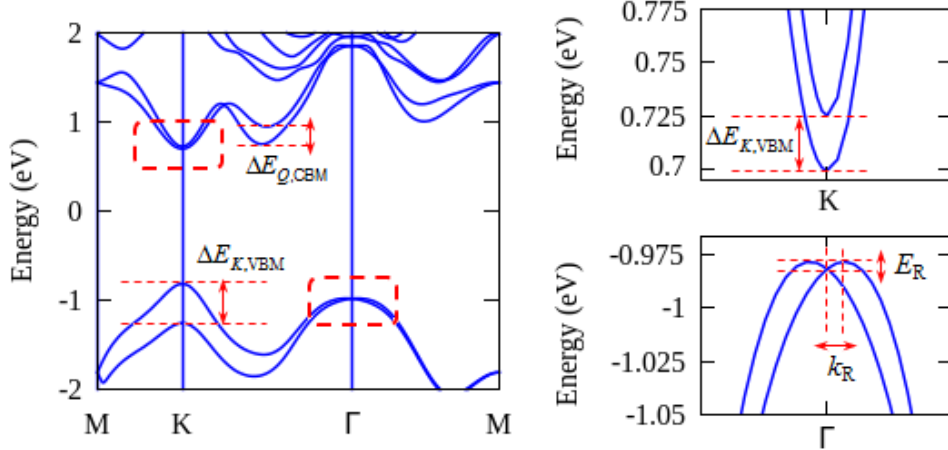


FIG. 2. The spin split bands in the polar WSe ML are given. The spin splitting in the K and Q are indicated by the red lines-arrows. The spin splitting around the Γ point known as Rashba splitting is highlighted, which is characterized by the Rashba energy (E_R), and momentum offset (k_R).

point is achieved, which is expected to play a significant role in the spintronics phenomena such as spin-conserving scattering.

B. Tunable the electronic and spin splitting properties by the strain

Because the polarity plays a significant role in the electronic and spin splitting properties of the TMDs ML, controlling the polarity is expected to induce useful properties for spintronics. Here, strain is an effective method to tune the polarity, which is achieved by applying substrates^{28,29,41}. To this aim, we use a wide range of biaxial strains (up to 8%) in the polar WSe ML by tuning the planar lattice parameter. The range of the strain considered in this work was chosen because the broken of inter-atomic bonds may occur for the larger strain. For example, in the MoS₂ ML, the breaking of the interatomic bonds is achieved at an effective strain of 6 to 11 %⁴². Because the WSe ML is polar material, the polar substrates having an intrinsic dipole moment such as wurtzite semiconductors²⁷ is suitable for inducing the strain. By choosing AlN as an example of the polar substrates ($a_0=3.11 \text{ \AA}$ ⁴³), a lattice constant mismatch of about 4.2 % is achieved on the interface of the polar WSe ML/AlN (0001), which is still within the range of the strain considered in

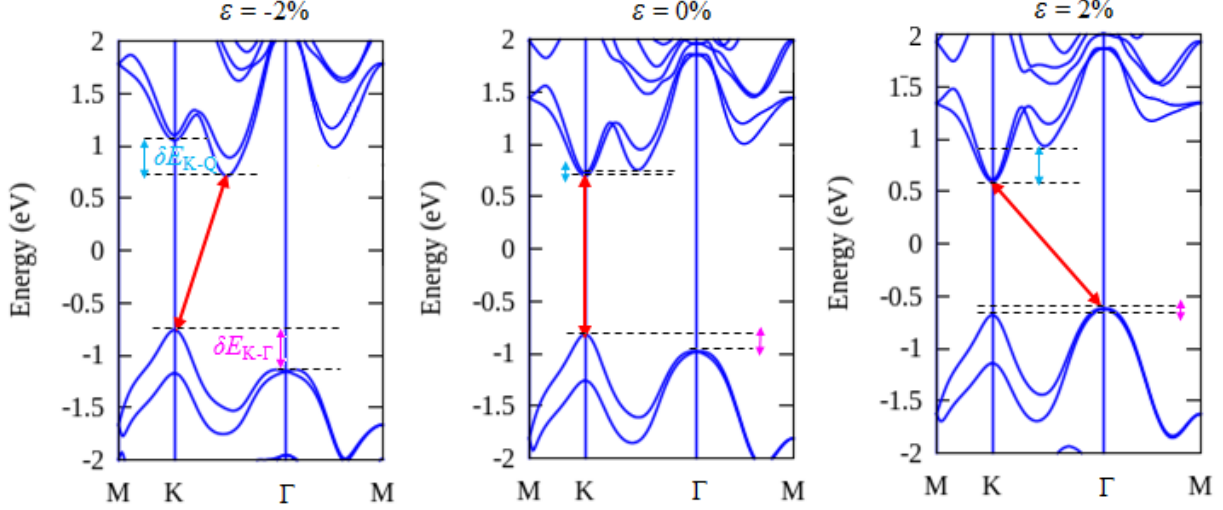


FIG. 3. Electronic band structures of the strained polar WSSe ML with $\epsilon = -2\%$ (left), $\epsilon = 0\%$ (center), and $\epsilon = 2\%$ (right) are given. The red, pink, and blue arrows indicate the band gap, energy difference between the K and Γ points ($\delta E_{K-\Gamma}$), and energy difference between the K and Q points (δE_{K-Q}), respectively. The calculations are performed by including the spin-orbit coupling.

the present study. We define the degree of in-plane biaxial strain as $\epsilon = (a - a_0)/a_0$, where a_0 is the unstrained in-plane lattice constant. Here, we studied the following two different cases: the tensile strain, which increases the in-plane lattice constant a , and compressive strain, which decreases a .

Under the tensile strain, we find that the out-of-plane interlayer distance difference Δd_{\perp} is decreased [Fig. 4(a)], and, consequently, the hybridization between the out-of-plane bonding states (d_{z^2}, p_z) is reduced, while the hybridization between the in-plane bonding states [$d_{x^2-y^2} + d_{xy}, S p_x + p_y$] is strengthened. As a result, energy level of the Γ point is higher than that of the K point in the VBM [Fig. 3]. On the other hand, the compressive strain shifts the energy level of the $d_{x^2-y^2} + d_{xy}$ anti-bonding states to be lower than that of the d_{z^2} anti-bonding states, resulting in that the energy level of the Q point is lower than that of the K point in the CBM. The shift of the energy level at the high symmetry points in the CBM and VBM by the strain has two important effects: (i) indirect band gap [Fig. 3], and (ii) the change of energy difference between the high symmetry points in the CBM and VBM [Fig. 4(b)]. We emphasized here that transition from the direct to the indirect band

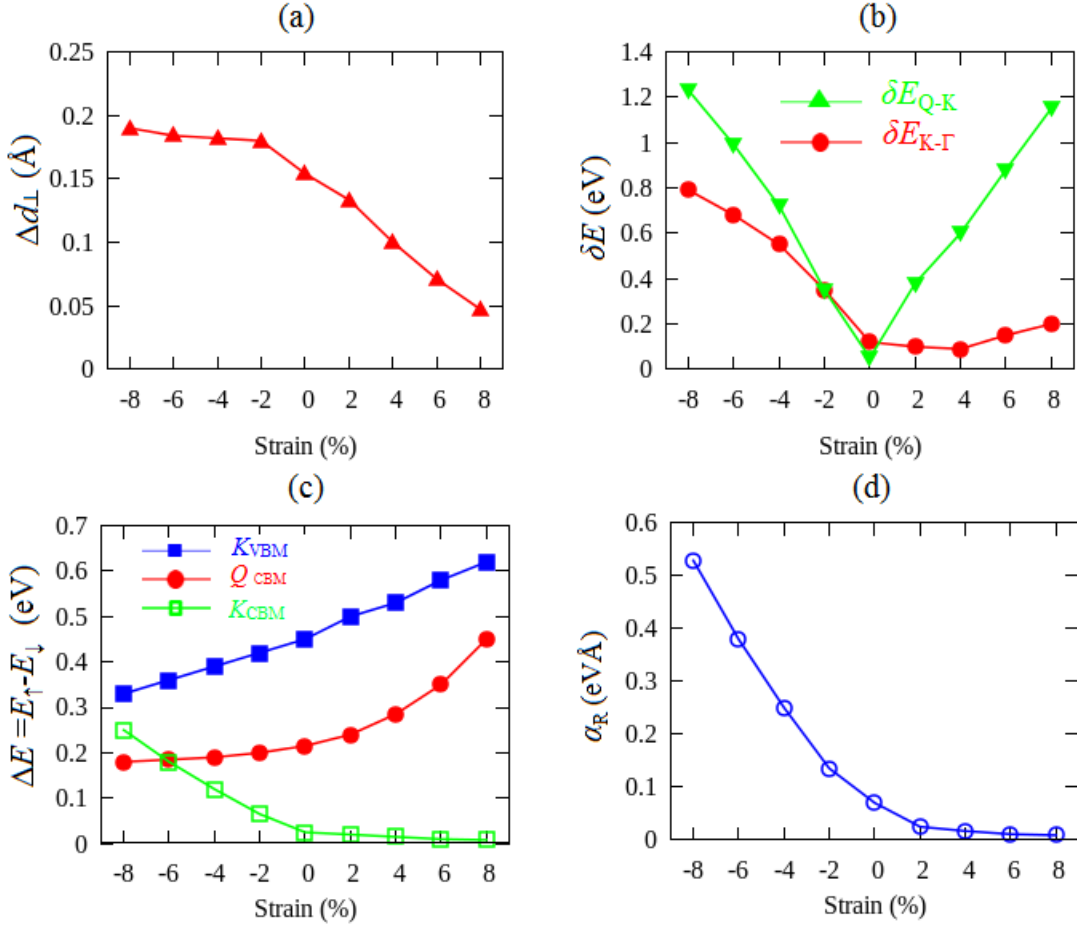


FIG. 4. (a) Strain-dependent of the out-of-plane interlayer distance difference (Δd_{\perp}) in the polar WSSe ML is shown. (b) The calculated value of the energy difference between the K and Γ points ($\delta E_{K-\Gamma}$) in the VBM, between the K and Q points in the CBM (δE_{K-Q}), and between the Q and Λ points in the CBM ($\delta E_{Q-\Lambda}$) as a function of strain. (c) Strain-dependent of the spin splitting energy $\Delta E = |E_{\uparrow} - E_{\downarrow}|$ at the high symmetry points in the CBM and VBM. (d) The Rashba parameter (α_R) as a function of strain, calculated around the Γ point in the VBM.

gap is achieved on a substantial critical strain, which is observed on -0.25 % and 1.9 % for the compressive and tensile strains, respectively. These values are slightly different from that seen on the non-polar WS_2 ML [(-1.2 % and 2.3 %) ¹⁷], but consistent with previous results reported by Defo *at. al.* ²⁷. Remarkably, tuning the polarity by the strain significantly modifies the electronic properties of the polar WSSe ML.

The strong modification of the electronic properties of the polar WSSe ML by the biaxial strain significantly changes the spin splitting properties of the bands. Due to the increased

overlap of the in-plane bonding states [$d_{x^2-y^2} + d_{xy}$, $S p_x + p_y$] by the tensile strain, strong enhancement of the spin splitting is observed on the K point in the VBM [Fig. 4(c)]. On the other hand, introducing the compressive strain increases the overlap of the out-of-plane bonding states (d_{z^2} , p_z), which contributes to the increasing of the spin splitting around the Γ point in the VBM [Fig. 2]. Consistently, the enhancement of the spin splitting is also identified in the CBM, which is observed on the Q point under the tensile strain, and on the K point under the compressive strain. These considerably changes of the spin splitting in the polar WSSe ML by applying the strain is expected to be useful for spintronics applications.

To better understand the nature of the observed spin splitting in the strained polar WSSe ML, we calculated the spin textures of the spin-split bands. Here, we focused on the spin textures in the VBM because of the enhanced spin splitting [Fig. 4(c)]. By considering the spin textures located on the 0.45 eV below the VBM, we find sixfold symmetry of spin-split hole pockets in the equilibrium as well as the strained systems. In the case of the equilibrium system, these hole pockets are clearly visible around the K point, exhibiting fully out-of-plane spin polarization [Fig. 5(b)]. On the other hand, the spin-split hole pockets show in-plane polarization around the Γ point, which is similar to the Rashba type spin textures²⁶. Introducing strain subsequently modifies the spin textures due to the shifting in energy of the VBM. In the case of the compressive strain, the energy level of the K point in the VBM is much higher than that of the Γ point, thus the spin textures is dominated by the out-of-plane polarization of the spin-split hole pockets around the K point [Fig. 5(a)]. On the contrary, in the case of the tensile strain, the energy level of the Γ point is close to that of the K point [Fig. 3], resulting in that the spin textures are characterized by the out-of-plane and in-plane polarizations of the spin-split hole pockets around the K and Γ points, respectively [Fig. 5(c)]. Because the energy difference between the K and Γ points is small [Fig. 4(b)], strong admixtures between the out-of-plane and in-plane spin polarized states are achieved, which is expected to influence the properties of spin relaxation and intervalley scattering times through the Dyakonov-Perel spin relaxation mechanism^{24,25}.

To clarify the origin of the observed spin splitting and the spin-polarized states in our calculational results, we consider our system based on the symmetry arguments. As mentioned before that the polar WSSe ML belongs to the C_{3v} symmetry group. Here, the symmetry itself consists of a C_3 rotation and a mirror symmetry operation $M_{y-z} : x \rightarrow -x$, where x is along the Γ - K direction. In the case of spin $\frac{1}{2}$ electrons, C_3 and M_{y-z} can be represented as

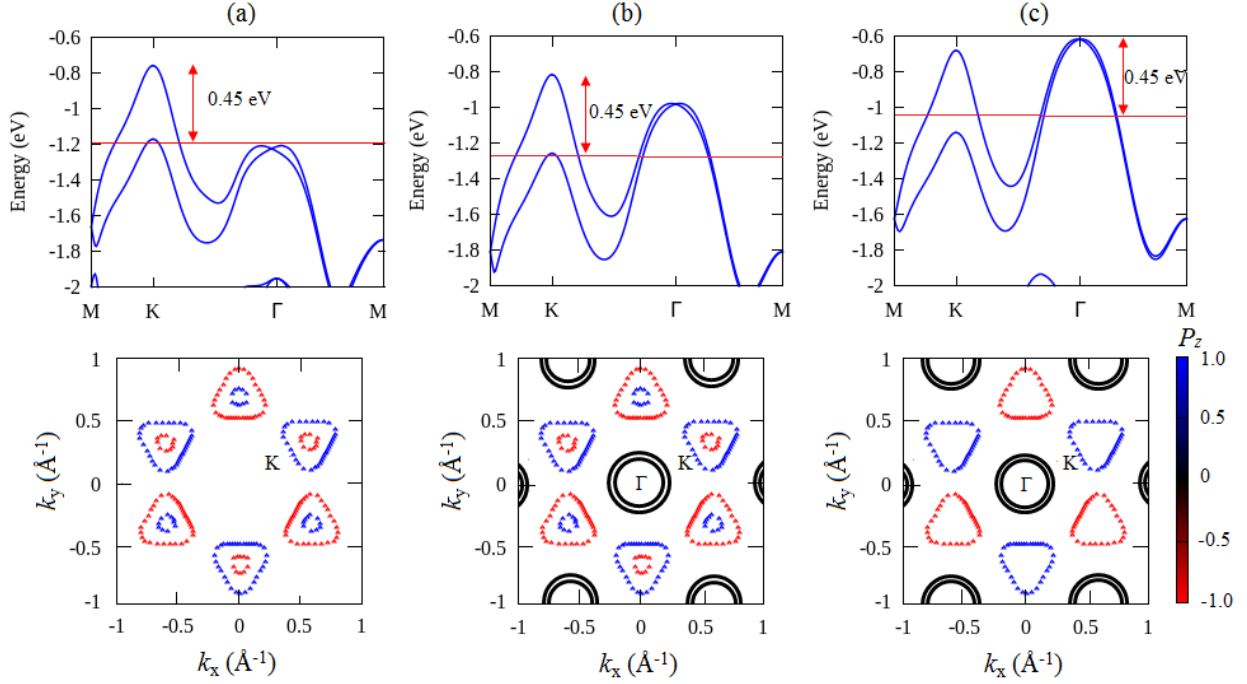


FIG. 5. The spin textures of the strained polar WSSe ML evaluated on the VBM: (a) $\epsilon = -2\%$, (b) $\epsilon = 0\%$, and (c) $\epsilon = 2\%$. The spin textures are calculated on the constant energy located on 0.45 eV below the VBM. The position of Γ and K points are indicated. Color scale shows expectation value of spin in the out-of-plane direction (P_z). Here, red and blue colors indicate the fully out-of-plane orientations of the spin-up ($P_z = 1$) and spin-down ($P_z = -1$) states, respectively, while the black colors indicate clock-wise and anti-clockwise in-plane orientations of the spin states ($P_z = 0$).

$\exp^{-i\sigma_z \frac{\pi}{3}}$ and $i\sigma_x$, respectively, where $\sigma_{x,y,z}$ are the Pauli matrices for spin degree of freedom. Additionally, the anti-unitary time reversal operator T that is represented by $i\sigma_y K$, where K is complex conjugation, commutes with both C_3 and M_{y-z} . The $\vec{k} \cdot \vec{p}$ Hamiltonian $H(\vec{k})$ up to cubic k -terms can be constructed around the Γ point by using invariant condition under C_3 , M_{y-z} , and T operations, which can be expressed as^{13,44,45}

$$H(\vec{k}) = E_0(k) + \alpha_R(k_x\sigma_y - k_y\sigma_x) + \beta_k(3k_x^2 - k_y^2)k_y\sigma_z, \quad (1)$$

where $E_0(k) = k^2/2m^*$ and $k = \sqrt{k_x^2 + k_y^2}$. Here, the second term in the $H(\vec{k})$ is the Rashba term characterized by Rashba parameter, α_R , which induces in-plane component of the spin polarization. On the other hand, the third term in the $H(\vec{k})$ is the warping term characterized by warping parameter, β_k , which contributes to the out-of-plane component of spin polarization. It is noted here that the Rashba parameter α_R is induced by out-of-plane

potential gradient asymmetry, while the warping parameter β_k is mainly contributed from in-plane potential gradient asymmetry. Solving the eigenvalues problem for the Hamiltonian of Eqs. (1) gives the following split energies:

$$E_{\pm}(k, \theta) = E_0(k) \pm \sqrt{\alpha_R^2 k^2 + \beta_k^2 k^6 \cos^2(3\theta)}, \quad (2)$$

where $\theta = \tan^{-1}(k_y/k_x)$ is the azimuth angle of momentum k with respect to the x axis along the Γ - K direction. The subscripts $+$ and $-$ denote states for the upper and lower bands, respectively. The spin polarization vector $\vec{P}_{\pm}(k, \theta)$ can be evaluated using the averaged components of the spin operator $\langle \vec{\sigma} \rangle$, which turns out to be

$$\vec{P}_{\pm}(k, \theta) = \pm[\alpha_R \sin \theta, -\alpha_R \cos \theta, -\beta_k \sin(3\theta)]. \quad (3)$$

In the case of the non-polar WS_2 ML, the mirror symmetry operation $M_{x-y} : z \rightarrow -z$ in the D_{3h} point group [Fig. 1(a)] suppresses the Rashba term in the $H(\vec{k})$, leading to the fact that only the third term in the Eq. (1) remains. As a result, zero spin splitting is observed at $\theta = n\pi/3$, where n is an integer number, which is consistent with the observed spin degeneracy in the band structures along the Γ - M direction shown in Fig. 2. However, the broken mirror symmetry M_{x-y} in the case of the polar WSSe ML lifts the spin degeneracy along the Γ - M [Fig. 2], which is due to the second term of the Eq. (1). Furthermore, due to the last term of the Eq. (3), fully-out-of plane spin polarization is visible at $\theta = (2n+1)\pi/6$, which is, in fact, consistent with our calculated results of the spin textures around the K point in the VBM [Fig. (5)]. However, the in-plane spin polarization is observed in the spin-split bands around the Γ point due to the first and second terms of Eq. (3), which is consistent with our results shown in Fig. 5. Therefore, it can be concluded that the spin splitting and spin textures in our calculational results are consistent well with the simplified Hamiltonian.

C. Discussion about possible application

Before continuing our discussion on possible spintronic applications of the enhanced spin splitting in the strained polar WSSe ML, we briefly comment on the seemingly spin splitting features around the Γ point in the VBM known as the Rashba splitting [see Fig. 2]. A comprehensive discussion of the Rashba splitting in the TMDs ML has been previously

presented by Cheng *at al.*²⁶. However, they have not considered the effect of the strain, which motivated us to extend their study. Naturally, the non-zero of Δd_{\perp} induces asymmetry of potential gradient perpendicular to the surface plane, leading to the strong hybridization between the out-of-plane bonding states $[d_{z^2}, p_z]$ in the Γ point. Consequently, the SOC leads to the Rashba spin splitting around the Γ point. However, decreasing (increasing) Δd_{\perp} by the compressive (tensile) strains [Fig. 4(a)], subsequently reduces (strengthens) the coupling between the out-of-plane bonding states, which decreases (increases) the Rashba splitting around the Γ point [Fig. 3]. The considerably changes of the Rashba splitting by the strain is in fact consistent with modulation of the Rashba parameter α_R shown in Fig. 4(d). It is noted here that the calculated value of α_R in the present system is obtained by using the linear Rashba model through relation defined by $\alpha_R = 2E_R/k_R$, where E_R and k_R are the Rashba energy and momentum offset, respectively. Here, E_R and k_R can be directly evaluated from the band dispersion obtained by the first-principles calculation [Fig. 2]. By analyzing the spin-split states given in Fig. 4, we found that $|\beta_k/\alpha_R| \approx 1\%$ for small k , indicating that the contribution of β_k to the spin splitting around the Γ point is negligible, which confirms a consistency of our calculational results. Finally, the observed Rashba splitting in the present work also supports the recent prediction of the Rashba splitting on strained MoS₂/Bi(111) heterostructures⁴⁶, where the broken of the mirror symmetry by the substrates plays an important role in generating the Rashba splitting in the various TMDs ML.

Here, we discuss the possible spintronic applications of the strained polar WSSe ML based on the features of the spin textures in the VBM. In the case of the equilibrium system, we found that the spin textures of the VBM are characterized by the out-of-plane and in-plane polarizations of the spin-split hole pockets around the K and Γ points, respectively [Fig. 5(b)]. These features of the spin textures are expected to induce spin-orbit field in the out-of-plane $B_{SO_{\perp}}$ and in-plane $B_{SO_{\parallel}}$ directions, respectively. The same orientation of the spin-orbit fields is also observed in the case of the tensile strain, which is due to the same features of the spin textures. Because the energy difference between the K and Γ points, $\delta E_{K-\Gamma}$, is small [Fig. 4(b)], strong admixtures between the out-of-plane and in-plane spin polarized states are achieved, leading to the fact that the coupling between $B_{SO_{\perp}}$ and $B_{SO_{\parallel}}$ around the K and Γ points, respectively, is strengthened. However, due to the substantially small spin splitting around the Γ point, weak in-plane spin-orbit field $B_{SO_{\parallel}}$ is generated,

inducing small misalignment of the total spin-orbit fields from the out-of-plane direction. Accordingly, Dyakonov-Perel spin relaxation mechanism implies that the spin relaxation times are much longer than that intervalley scattering times. This situation is qualitatively similar to the recent observation of the spin relaxation on dual gated exfoliated MoS₂ ML reported by Schmidt *at al.*²⁴, which found that applying ionic gating breaks the mirror symmetry to induces the enhanced spin relaxation.

Interestingly, the spin textures of the VBM in the case of the compressive strain is dominated by the fully out-of-plane polarization of the spin-split hole pockets around the K point [Fig. 5(a)]. Here, the fully out-of-plane orientation of the spin-orbit fields $B_{SO_{\perp}}$ is generated, implying that unusually long spin relaxation times without intervalley scattering is achieved. This is supported by the fact that a similar mechanism behind the long spin relaxation times induced by out-of-plane spin polarization has been reported on the various TMDs ML^{14,17,24,25,47}, suggesting that the present system is promising for energy saving spintronics.

It is pointed out here that our proposed approach for generating and modulating the spin splitting and spin-polarized states is not limited to the polar WSSe ML, but it can be generalized to a variety of SOC systems with the polar MXY structures exhibiting the polarity-induced mirror symmetry breaking (for example, other the polar TMDS ML including WSTe, MoSSe and MoSTe whose electronic structure properties are similar to WSSe ML^{26,27}). Together, these features seem to be promising for inducing new electronic properties which are useful for spintronic applications.

IV. CONCLUSION

To summarize, we have investigated the effect of the polarity and its strain dependent on the electronic properties of the TMDs ML by using first-principles density functional theory calculations. We found that in addition to the established spin splitting along the Γ - K line with fully-out-of-plane spin polarization, the presence of the mirror symmetry breaking in the polar TMDs ML leads to sizable spin splitting along the Γ - M line exhibiting in-plane spin polarization. We also find that these splittings are effectively controlled by tuning the polarity realized by introducing biaxial strain. We clarified the origin of the spin splitting and spin polarization in our calculational results by using symmetry arguments combined

with orbital hybridization analyses. The enhanced and sizable spin splittings found in the present study suggested that the strained polar TMDs ML systems are suitable for spintronic applications. Finally, we have identified the possible admixtures of the out-of-plane and in-plane spin-polarized states in the strained polar systems and discussed their implications to the spin relaxation involving intervalley scattering process through the Dyakonov-Perel mechanism. Our study clarified that the polarity-induced mirror symmetry breaking is an important parameter to control the spin splitting and spin relaxation in the TMDs ML, which is useful for designing future spintronic devices.

ACKNOWLEDGMENTS

This work was supported by the Fundamental Reserach Grant (2017) funded by the ministry of research and technolgy and higher eduacation, Republic of Indonesia. The computations in this research were performed using the high performance computing facilities (DSDI) at Universitas Gadjah Mada, Indonesia.

REFERENCES

- ¹Y. Kato, R. C. Myers, A. C. Gossard, and D. D. Awschalom, “Coherent spin manipulation without magnetic fields in strained semiconductors,” *Nature* **427**, 50 (2004).
- ²S. Kuhlen, K. Schmalbuch, M. Hagedorn, P. Schlammes, M. Patt, M. Lepsa, G. Güntherodt, and B. Beschoten, “Electric field-driven coherent spin reorientation of optically generated electron spin packets in ingaas,” *Phys. Rev. Lett.* **109**, 146603 (2012).
- ³X.-L. Qi, Y.-S. Wu, and S.-C. Zhang, “Topological quantization of the spin hall effect in two-dimensional paramagnetic semiconductors,” *Phys. Rev. B* **74**, 085308 (2006).
- ⁴S. Datta and B. Das, “Electronic analog of the electrooptic modulator,” *Appl. Phys. Lett.* **56**, 665–667 (1990).
- ⁵J. Nitta, T. Akazaki, H. Takayanagi, and T. Enoki, “Gate control of spin-orbit interaction in an inverted $\text{In}_{0.53}\text{Ga}_{0.47}\text{As}/\text{In}_{0.52}\text{Al}_{0.48}\text{As}$ heterostructure,” *Phys. Rev. Lett.* **78**, 1335–1338 (1997).
- ⁶K. S. Novoselov, A. K. Geim, S. V. Morozov, D. Jiang, Y. Zhang, S. V. Dubonos, I. V. Grigorieva, and A. A. Firsov, “Electric field effect in atomically thin carbon films,” *Science*

- 306**, 666 (2004).
- ⁷S. Cahangirov, M. Topsakal, E. Aktürk, H. Şahin, and S. Ciraci, “Two- and one-dimensional honeycomb structures of silicon and germanium,” *Phys. Rev. Lett.* **102**, 236804 (2009).
- ⁸H. Min, J. E. Hill, N. A. Sinitsyn, B. R. Sahu, L. Kleinman, and A. H. MacDonald, “Intrinsic and rashba spin-orbit interactions in graphene sheets,” *Phys. Rev. B* **74**, 165310 (2006).
- ⁹C.-C. Liu, W. Feng, and Y. Yao, “Quantum spin hall effect in silicene and two-dimensional germanium,” *Phys. Rev. Lett.* **107**, 076802 (2011).
- ¹⁰C. L. Kane and E. J. Mele, “Quantum spin hall effect in graphene,” *Phys. Rev. Lett.* **95**, 226801 (2005).
- ¹¹D. Xiao, G.-B. Liu, W. Feng, X. Xu, and W. Yao, “Coupled spin and valley physics in monolayers of mos_2 and other group-vi dichalcogenides,” *Phys. Rev. Lett.* **108**, 196802 (2012).
- ¹²X. D. Xu, W. Yao, D. Xiao, and T. F. Heinz, “Spin and pseudospins in layered transition metal dichalcogenides,” *Nat. Physics* **10**, 343 (2014).
- ¹³H. Yuan, M. S. Bahramy, K. Morimoto, S. Wu, K. Nomura, B.-J. Yang, H. Shimotani, R. Suzuki, M. Toh, C. Kloc, X. Xu, R. Arita, N. Nagaosa, and Y. Iwasa, “Zeeman-type spin splitting controlled by an electric field,” *Nat. Physics* **9**, 563 (2013).
- ¹⁴Z. Y. Zhu, Y. C. Cheng, and U. Schwingenschlögl, “Giant spin-orbit-induced spin splitting in two-dimensional transition-metal dichalcogenide semiconductors,” *Phys. Rev. B* **84**, 153402 (2011).
- ¹⁵D. W. Latzke, W. Zhang, A. Suslu, T.-R. Chang, H. Lin, H.-T. Jeng, S. Tongay, J. Wu, A. Bansil, and A. Lanzara, “Electronic structure, spin-orbit coupling, and interlayer interaction in bulk mos_2 and ws_2 ,” *Phys. Rev. B* **91**, 235202 (2015).
- ¹⁶G.-B. Liu, W.-Y. Shan, Y. Yao, W. Yao, and D. Xiao, “Three-band tight-binding model for monolayers of group-vib transition metal dichalcogenides,” *Phys. Rev. B* **88**, 085433 (2013).
- ¹⁷M. A. U. Absor, H. Kotaka, F. Ishii, and M. Saito, “Strain-controlled spin splitting in the conduction band of monolayer ws_2 ,” *Phys. Rev. B* **94**, 115131 (2016).
- ¹⁸R.-L. Chu, X. Li, S. Wu, Q. Niu, W. Yao, X. Xu, and C. Zhang, “Valley-splitting and valley-dependent inter-landau-level optical transitions in monolayer mos_2 quantum hall

- systems,” *Phys. Rev. B* **90**, 045427 (2014).
- ¹⁹R. A. Bromley, R. B. Murray, and A. D. Yoffe, “The band structures of some transition metal dichalcogenides. iii. group via: trigonal prism materials,” *Journal of Physics C: Solid State Physics* **5**, 759 (1972).
- ²⁰K. Kośmider, J. W. González, and J. Fernández-Rossier, “Large spin splitting in the conduction band of transition metal dichalcogenide monolayers,” *Phys. Rev. B* **88**, 245436 (2013).
- ²¹M. A. Cazalilla, H. Ochoa, and F. Guinea, “Quantum spin hall effect in two-dimensional crystals of transition-metal dichalcogenides,” *Phys. Rev. Lett.* **113**, 077201 (2014).
- ²²Y. Ma, L. Kou, X. Li, Y. Dai, S. C. Smith, and T. Heine, “Quantum spin hall effect and topological phase transition in two-dimensional square transition-metal dichalcogenides,” *Phys. Rev. B* **92**, 085427 (2015).
- ²³Z. Gong, G.-B. Liu, H. Yu, D. Xiao, X. Cui, X. Xu, and W. Yao, “Magnetoelectric effects and valley-controlled spin quantum gates in transition metal dichalcogenide bilayers,” *Nat. Commun.* **4**, 2053 (2013).
- ²⁴H. Schmidt, I. Yudhistira, L. Chu, A. H. Castro Neto, B. Özyilmaz, S. Adam, and G. Eda, “Quantum transport and observation of dyakonov-perel spin-orbit scattering in monolayer mos₂,” *Phys. Rev. Lett.* **116**, 046803 (2016).
- ²⁵L. Yang, N. A. Sinitsyn, W. Chen, J. Yuan, J. Zhang, J. Lou, and S. A. Crooker, “Long-lived nanosecond spin relaxation and spin coherence of electrons in monolayer mos₂ and ws₂,” *Nat. Physics* **11**, 830 (2015).
- ²⁶Y. C. Cheng, Z. Y. Zhu, M. Tahir, and U. Schwingenschlgl, “Spin-orbitinduced spin splittings in polar transition metal dichalcogenide monolayers,” *EPL* **102**, 57001 (2013).
- ²⁷R. K. Defo, S. Fang, S. N. Shirodkar, G. A. Tritsarlis, A. Dimoulas, and E. Kaxiras, “Strain dependence of band gaps and exciton energies in pure and mixed transition-metal dichalcogenides,” *Phys. Rev. B* **94**, 155310 (2016).
- ²⁸E. Xenogiannopoulou, P. Tsipas, K. E. Aretouli, D. Tsoutsou, S. A. Giamini, C. Bazioti, G. P. Dimitrakopoulos, P. Komninou, S. Brems, C. Huyghebaert, I. P. Radu, and A. Dimoulas, “High-quality, large-area mose₂ and mose₂/bi₂se₃ heterostructures on aln(0001)/si(111) substrates by molecular beam epitaxy,” *Nanoscale* **7**, 7896 (2015).
- ²⁹K. E. Aretouli, P. Tsipas, D. Tsoutsou, J. Marquez-Velasco, E. Xenogiannopoulou, S. A. Giamini, E. Vassalou, N. Kelaidis, and A. Dimoulas, “Two-dimensional semiconductor

- hfse2 and mose2/hfse2 van der waals heterostructures by molecular beam epitaxy,” *Applied Physics Letters* **106**, 143105 (2015).
- ³⁰J. P. Perdew, K. Burke, and M. Ernzerhof, “Generalized gradient approximation made simple,” *Phys. Rev. Lett.* **77**, 3865–3868 (1996).
- ³¹T. Ozaki, H. Kino, J. Yu, M. J. Han, N. Kobayashi, M. Ohfuti, F. Ishii, T. Ohwaki, H. Weng, and K. Terakura, <http://www.openmx-square.org/>.
- ³²N. Troullier and J. L. Martins, “Efficient pseudopotentials for plane-wave calculations,” *Phys. Rev. B* **43**, 1993–2006 (1991).
- ³³T. Ozaki, “Variationally optimized atomic orbitals for large-scale electronic structures,” *Phys. Rev. B* **67**, 155108 (2003).
- ³⁴T. Ozaki and H. Kino, “Numerical atomic basis orbitals from h to kr,” *Phys. Rev. B* **69**, 195113 (2004).
- ³⁵H. Kotaka, F. Ishii, and M. Saito, “Rashba effect on the structure of the bi one-bilayer film: Fully relativistic first-principles calculation,” *Jpn. J. Appl. Phys.* **52**, 035204 (2013).
- ³⁶M. A. U. Absor, H. Kotaka, F. Ishii, and M. Saito, “Tunable rashba effect on strained zno: First-principles density-functional study,” *Applied Physics Express* **7**, 053002 (2014).
- ³⁷M. A. U. Absor, F. Ishii, H. Kotaka, and M. Saito, “Persistent spin helix on a wurtzite zno (10 $\bar{1}$ 0) surface: First-principles density-functional study,” *Applied Physics Express* **8**, 073006 (2015).
- ³⁸M. A. U. Absor, F. Ishii, H. Kotaka, and M. Saito, “Spin-split bands of metallic hydrogenated zno (1010) surface: First-principles study,” *AIP Advances* **6**, 025309 (2016).
- ³⁹D. M. Guzman and A. Strachan, “Role of strain on electronic and mechanical response of semiconducting transition-metal dichalcogenide monolayers: An ab-initio study,” *Journal of Applied Physics* **115**, 243701 (2014).
- ⁴⁰A. Kormnyos, G. Burkard, M. Gmitra, J. Fabian, V. Zlyomi, N. D. Drummond, and V. Falko, “k p theory for two-dimensional transition metal dichalcogenide semiconductors,” *2D Materials* **2**, 022001 (2015).
- ⁴¹T. Brumme, M. Calandra, and F. Mauri, “First-principles theory of field-effect doping in transition-metal dichalcogenides: Structural properties, electronic structure, hall coefficient, and electrical conductivity,” *Phys. Rev. B* **91**, 155436 (2015).
- ⁴²S. Bertolazzi, J. Brivio, and A. Kis, “Stretching and breaking of ultrathin mos2,” *ACS Nano* **5**, 9703–9709 (2011), PMID: 22087740.

- ⁴³D. Nilsson, E. Janzn, and A. Kakanakova-Georgieva, “Lattice parameters of aln bulk, homoepitaxial and heteroepitaxial material,” *Journal of Physics D: Applied Physics* **49**, 175108 (2016).
- ⁴⁴L. Fu, “Hexagonal warping effects in the surface states of the topological insulator bi_2te_3 ,” *Phys. Rev. Lett.* **103**, 266801 (2009).
- ⁴⁵S. Vajna, E. Simon, A. Szilva, K. Palotas, B. Ujfalussy, and L. Szunyogh, “Higher-order contributions to the rashba-bychkov effect with application to the $\text{bi}/\text{ag}(111)$ surface alloy,” *Phys. Rev. B* **85**, 075404 (2012).
- ⁴⁶K. Lee, W. S. Yun, and J. D. Lee, “Giant rashba-type splitting in molybdenum-driven bands of $\text{mos}_2/\text{Bi}(111)$ heterostructure,” *Phys. Rev. B* **91**, 125420 (2015).
- ⁴⁷H. Liu, J. Chen, H. Yu, F. Yang, L. Jiao, G.-B. Liu, W. Ho, C. Gao, J. Jia, W. Yao, and M. Xie, “Observation of intervalley quantum interference in epitaxial monolayer tungsten diselenide,” *Nat. Commun* **6**, 8180 (2015).